ICAS 2016
30th Congress of the International Council of the Aeronautical Sciences
DCC, Daejeon, Korea ; September 25-30, 2016

DEVELOPMENT OF A THREE-DIMENSIONAL TIGHTLY COUPLED EULER/POTENTIAL FLOW SOLVER FOR TRANSONIC FLOW

Yeongmin Jo*†, Se Hwan Park*, Duck-Joo Lee*, and Seongim Choi††
***Korea Advanced Institute of Science and Technology, Daejeon, 34141, South Korea**
††Virginia Polytechnic Institute and State University, Blacksburg, 24060, United States
†yminjo@kaist.ac.kr

Abstract

The purpose of the current study is to develop an efficient yet accurate two-way coupling method integrating Euler and potential flow solvers for transonic flow simulations. An artificial boundary condition is introduced which reduce a CFD domain size, and the disturbed flow properties near a body is represented by the potential flow solver. On the other hand, the linear potential flow solution is updated by the Euler solver to incorporate the nonlinear shock phenomena into the solution. The tightly coupled solver is validated in various flow conditions as subsonic and transonic flows around two-dimensional airfoil and three-dimensional wings. The validation results showed that the tightly coupled solver can improve the efficiency with good accuracy compared to a conventional Euler solver.

1 Introduction

A linear potential flow solver has been widely used in industries in several decades because it is a fast method to compute both incompressible and compressible flows with little nonlinear flow phenomena reasonably well. However, it may inaccurate when the flow viscosity cannot be negligible, or the nonlinearity of the flow is dominant. In that case, more complex computation methods such as the Euler or Navier-Stokes (N-S) equations are needed, but they require much computation time. Thus, the computation accuracy and the time are always traded off.

There have been attempts to adopt the advantages of the various computation methods. Sankar et al.[1] developed a hybrid solver by coupling the N-S solver with the full potential solver for a viscous flow solution. They divided a flow domain into inner viscous flow region for the N-S solver and outer irrotational flow region for the potential flow solver to reduce the computation time. Srinivasan et al.[2] and Khanna et al.[3] coupled a free-wake model to the Euler and N-S solvers to accurately modelling vortices leaving the viscous flow region without numerical dissipation. Wie et al.[4] developed a hybrid solver for helicopter rotor flows by coupling the potential flow solver, the N-S solver, and the free-wake model.

In a typical CFD computation for external flows, a far-field boundary condition is widely used. It is based on a physical nature that disturbed (perturbed) flows after flowing objects diminish and it return to the freestream condition on the CFD domain boundary. Correspondingly, the domain boundary size has to be large enough, which makes the CFD computation being inefficient.

In the current study, we develop a two-way tightly coupled Euler and linear potential flow solver for transonic flows to improve the efficiency with good accuracy compared to a conventional Euler solver. For that coupling, a small CFD domain boundary as an artificial boundary is defined, which its size is as small as that the flow disturbances need to be considered. The disturbances are numerically calculated by the linear potential flow solver and with other equations of the flow physics. However, the linear potential flow solver cannot solve the transonic flows with nonlinear shock waves. To overcome that point, the Euler solver serves

discontinuous solutions to the potential solver, the potential solver can consider the nonlinear flows. Thus, the two solvers in a complementary relation.

This paper is organized as follow. First, the governing equations of the Euler and potential flow solutions are described, mathematical formulations for the coupling process are derived, and the coupling process is explained in Sec. 2. After that, the efficiency of the tightly coupled solver is validated in various flow cases as the subsonic and transonic flows around two-dimensional airfoil and three-dimension wings in Sec. 3. Finally, this paper is concluded with the conclusions and future work in Sec. 4.

2 Coupling Methodology

In this section, the governing equations of the Euler and potential flow are explained. Based on the equations, an update method of the flow properties for both solvers is introduced.

2.1 Euler Solver

Semi-discretized, integral form of three-dimensional Euler equations are described in Eq. 1.

$$\int_{\Omega_i} \frac{\partial \boldsymbol{U}}{\partial t} d\Omega + \sum_{j \in N_i} F_{ij}^c \Delta S_{ij} - \boldsymbol{Q}|\Omega_i| = 0 \quad (1)$$

where $\boldsymbol{U}$ is the vector of state variables, F_{ij}^c is a convective flux term, $\boldsymbol{Q}$ is a source term. ΔS_{ij} is the area of the face edge between ith and jth control volumes when Ω_i is the ith control volume, and N_i is defines the set of neighboring nodes for ith node. For the Euler computation, the CFD solver of SU2_CFD [5] code is used. This solver is a programming software to solve finite volume based flow governing equations of Euler, Navier-Stokes, Reynolds averaged Navier-Stokes (RANS), Poisson, heat, wave, etc. In addition, it can also simulate high-fidelity multi-physics such as fluid-structure interaction, non-equilibrium flow, etc. Furthermore, it solves continuous and discrete adjoint solutions for efficient gradient evaluations. In the current study, Jameson-Schmidt-Turkel (JST) scheme and Euler implicit scheme with lower-upper symmetric gauss-seidel method (LU-SGS) are used for the spatial discretization and the time integration. SU2_CFD serves agglomeration multi-grid method for fast convergence, but it is not used for the fair comparison of the computation time.

2.2 Linear Potential Flow Solver

Three-dimensional linearized compressible potential flow equation is described in Eq. 2.

$$\beta \phi_{xx} + \phi_{yy} + \phi_{zz} = 0 \quad (2)$$

where $\beta = 1 - M_\infty^2$ is a compressibility factor and ϕ is a velocity potential. In the current study, Vortexje [6] code is used. This is based on low-order panel method with source and doublet elements. Because the code solves incompressible flow only, the compressibility effect is implemented. A general solution of Eq. 2 is the Green's function in Eq. 3.

$$\begin{aligned} \phi = \phi' + \phi_\infty = & \frac{1}{4\pi} \int_{b+w} \mu \frac{\partial}{\partial n} \left(\frac{1}{r}\right) dS \\ & - \frac{1}{4\pi} \int_b \sigma \left(\frac{1}{r}\right) dS \\ & + \phi_\infty \end{aligned} \quad (3)$$

where ϕ, ϕ', and ϕ_∞ are the total velocity potential, perturbed velocity potential, and the freestream velocity potential, respectively. The subscript b and w represent the body surface panels and wake sheets, and μ and σ are the doublet and source strengths, respectively. r is the Euclidean distance with the compressibility effect between ith surface panel (of wake sheet) and a location in velocity field defined in Eq. 4.

$$r = \sqrt{(x - x_i)^2 + \beta[(y - y_i)^2 + (z - z_i)^2]} \quad (4)$$

Two types of Neumann boundary condition are needed to solve Eq. 2. The first is a far-field boundary condition describing that the flow perturbation diminish at the far field, which is described in Eq. 5.

$$\lim_{r \to \infty} \nabla \phi' = 0 \quad (5)$$

This condition is automatically satisfied as ϕ' goes zero exponentially as r increases. The

second is solid boundary condition that the velocity normal to the surface panel should be zero, which is described in Eq. 6.

$$\nabla(\phi' + \phi_\infty) \cdot \vec{n}_i = 0 \qquad (6)$$

where $\vec{n}_i$ is the normal vector of i[th] body surface panel. This equation is equivalent to Eq. 7.

$$\sigma_i = -\frac{\partial \phi}{\partial n_i} = \vec{v}_\infty \cdot \vec{n}_i \qquad (7)$$

which means that each source strength can be explicitly determined by the normal vector and the freestream velocity.

The doublet strength of each wake sheet is determined with a physical flow condition of the Kutta condition in Eq. 8.

$$\mu_i^w = \mu_{i,upper}^b - \mu_{i,lower}^b \qquad (8)$$

where $\mu_{i,upper}^b$ and $\mu_{i,lower}^b$ are the doublet strengths of adjacent upper and lower body surface panels of the i[th] wake panel. Finally, the doublet strengths of the body surface panels are determined implicitly by an iterative numerical computation, and the velocity induced by the potential flow solution at any location *(x,y,z)* in the flow field is calculated by differentiate Eq. 3 as $\vec{v}(x, y, z) = \nabla\phi$.

2.3 Updates of Flow Properties

In order to serve the perturbed flow properties at an artificial boundary for the Euler solver, we use not only the potential flow solution, but also the compressible Bernoulli equation and the isentropic relation in Eq. 9 and Eq. 10.

$$\frac{\gamma}{\gamma - 1}\frac{p}{\rho} + \frac{|v|^2}{2} = \frac{\gamma}{\gamma - 1}\frac{p_\infty}{\rho_\infty} + \frac{|v_\infty|^2}{2} \qquad (9)$$

$$\frac{p}{p_\infty} = \left(\frac{\rho}{\rho_\infty}\right)^\gamma \qquad (10)$$

Thus, the pressure and density are calculated simultaneously when the velocity is calculated by the potential flow solution.

In the tightly coupling process, the doublet strengths for the potential flow solution are updated by the computed Euler solution. As opposite direction of the above calculation sequence, a representative flow velocity is calculated using the pressure and density properties from the Euler solution. Because the Euler solution assumes there is no flow separation, the flow velocity can be approximated to the tangential velocity. Then the perturbed velocity is calculated by subtracting the freestream velocity from the tangential velocity as $|\vec{v}'| = [v] - |v_\infty|$. Finally, the surface doublet is computed by integrating the perturbed velocity along the body surface as Eq. 11.

$$\mu(x) = -\int_{T.E.}^{x} |\vec{v}'| dl \qquad (11)$$

where *T.E.* means the trailing edge, and *x* is an arbitrary location on the body surface, and *dl* is a unit length for the integration.

The above update method is validated. Fig. 1 shows the doublet strength on the surface of NACA 0012 airfoil calculated by the coupled solver (red line) and the conventional potential flow solver (blue dots). The flow condition is Mach number of $\mathbf{M = 0.2}$ at angle of attack of $\boldsymbol{\alpha = 5°}$. As shown in the figure, the update method is very accurate compared to the potential flow solution.

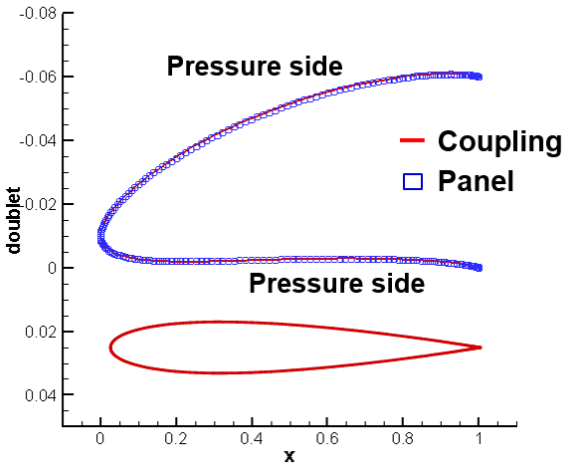

Fig. 1 Comparison of doublet strength for validation ($\mathbf{M = 0.2}$, $\boldsymbol{\alpha = 5°}$)

2.4 Tightly Coupling Process

The tightly coupling process starts from initial solving the potential solution. Then the induced velocity on an artificial boundary is

calculated from the solution, and corresponding the pressure density are calculated by the compressible Bernoulli equation in Eq. 9 and the isentropic relation in Eq. 10. Using the perturbed flow properties, the Euler solver computes a transonic nonlinear flow solution iteratively. After obtaining a converged solution, the surface doublet is calculated by Eq. 11 with the Euler solution, and the initial potential flow solution is updated. This process goes iteratively until a converged solution is obtained. This process is illustrated in Fig. 2.

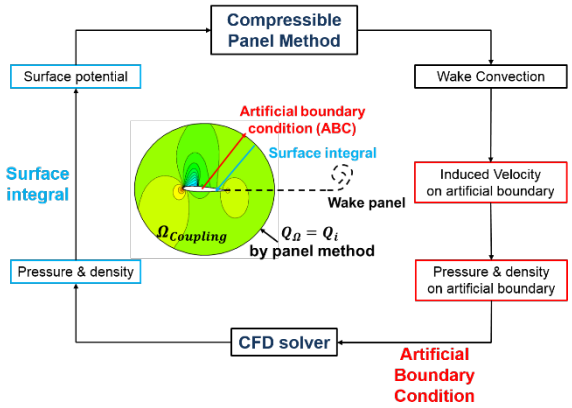

Fig. 2 Schematic of tightly coupling process

3 Validation

In this section, the tightly coupled solver is validated in various flow cases. First, the subsonic and transonic flows around a two-dimensional NACA 0012 airfoil are computed. In three-dimensional flow cases, a NACA 23012 rectangular wing and ONERA m6 swept wing are used for the subsonic and transonic flows, respectively. In each case, we focus on to compare the computation time of the tightly coupled solver with that of the conventional Euler solver to investigate how much the tightly coupled solver is efficient.

3.1 Two-Dimensional NACA 0012 Airfoil at Subsonic Flow (M = 0.1, α = 3°)

The first case was the two-dimensional NACA 0012 at the subsonic flow. The flow condition was Mach number of M = 0.1 at angle of attack of α = 3°. For the CFD computation, C-type of structured grids with different domain size were generated. The domain size was controlled by a distance parameter defined in unit length of the airfoil chord, and the parameter defines the distance between the airfoil surface and the domain boundary. Fig. 3 shows a schematic of the domain size parameterization, and examples of the grids with the domain size of 50, 1, and 0.1 chord lengths are shown in Fig. 4.

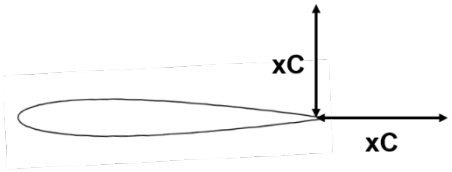

Fig. 3 Schematic of domain size parameterization

The computation results of the tightly coupled solver and the conventional Euler solver were compared in terms of the lift coefficient in Fig. 5 and the computation time in Fig. 6. In comparison of the lift coefficient, the reference was the Euler solver with very large domain size of 500 chord length. It is confirmed that, the coupled solver with small domain size of 0.1 chord length shows very accurate results as the error was 1.67% less than 2%.

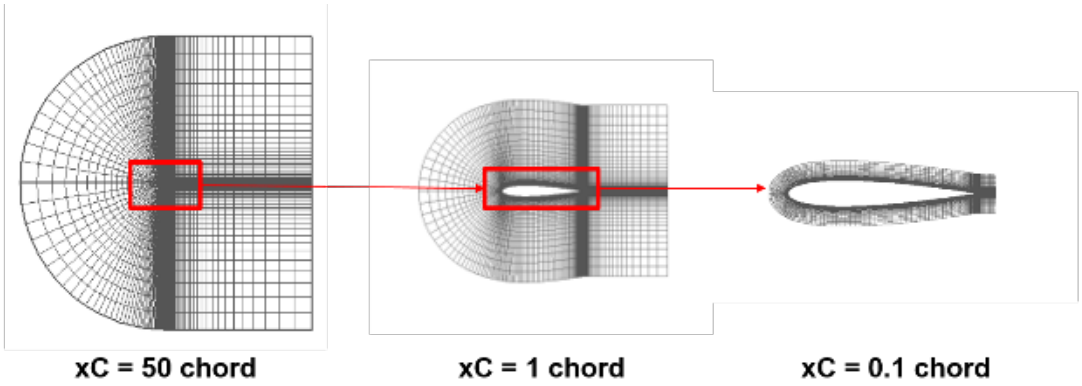

Fig. 4 Examples of grids with different domain sizes

In comparison of the computation time, the reference was the Euler solver with domain size of 50 chord length. In Fig. 6, it is validated that the tightly coupled solver reduced the computation time considerably as ratio of the computation time between the coupled solver and the reference was about 1/7.

Fig. 7 shows the surface pressure distribution between the results of the tightly coupled solver with domain size of 0.1 chord length (red dots) and that of the Euler solver with domain size of 500 chord length (black line). This figure demonstrates that how much the tightly coupled solver is accurate even with very small domain size as the two distributions showed excellent agreement with each other.

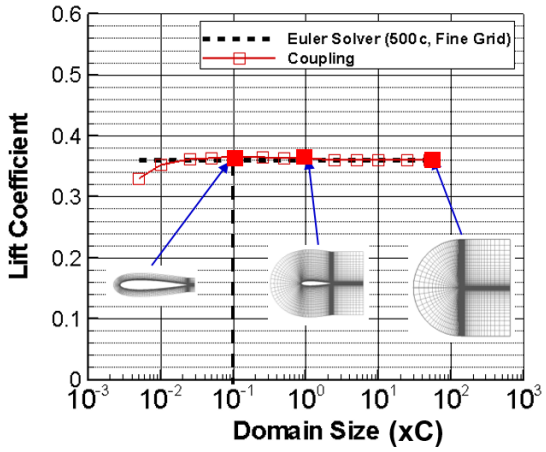

Fig. 5 Lift coefficient along domain size

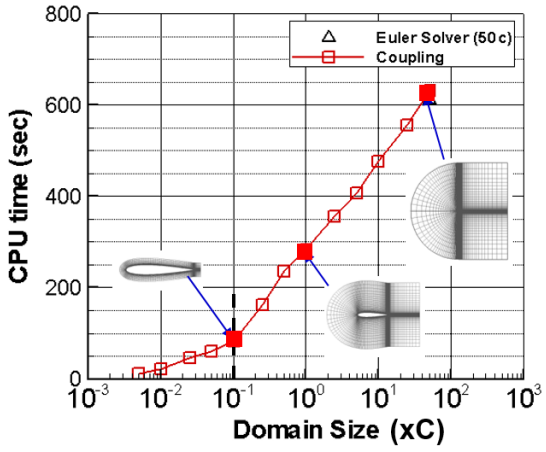

Fig. 6 Computation time along domain size

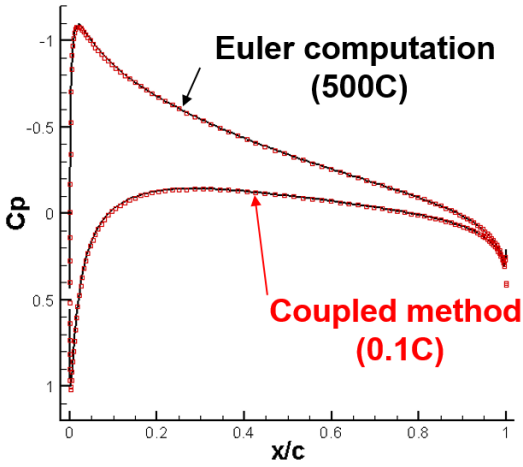

Fig. 7 Comparison of surface pressure distribution

3.2 Two-Dimensional NACA 0012 Airfoil at Transonic Flow ($M = 0.7$, $\alpha = 3°$)

The second case was the transonic flow with the same airfoil. The flow condition was Mach number of $M = 0.7$ at angle of attack of $\alpha = 3°$ which generates nonlinear shock waves on the upper surface. The same grids described in the previous section were used. For each comparison, the references were the same as that in the previous section.

Fig. 8 shows the lift coefficient along the domain size. In contrast with the previous case, the tightly coupled solver with the small domain size became inaccurate, as the error were 10% and 3% with the domain sizes of 0.1 and 1 chord lengths, respectively. However, the coupled solver with the larger domain size as 2.5 chord length showed good accuracy with the error of 1.78%. Correspondingly, the ratio of the computation time was about 1/3 in Fig. 9.

Fig. 10 shows the surface pressure distributions. It is confirmed that the shock position and the strength were well predicted by the tightly coupled solver with the small domain size. Correspondingly, Fig. 11 shows the pressure fields computed by the tightly coupled solver with the domain size and the reference. The two fields look very similar with each other, even in the strong shock region.

Returning to the inaccuracy issue with the small domain sizes, it can be construed that although the surface doublet strengths of the

potential flow solver are updated from the nonlinear Euler solution, the induced velocities on the artificial boundary are propagated by the linear governing equation. In addition, the propagation will be more inaccurate when the velocity propagates across the supersonic region which has completely different flow governing characteristics. These limitations will be investigated in detail and an appropriate method will be devised to overcome them. However, the tightly coupled solver is still valid even with the limitations.

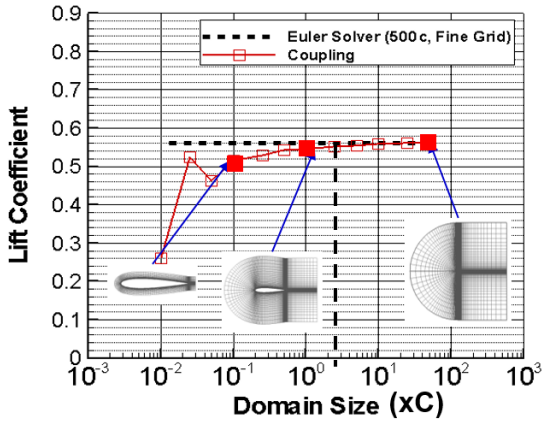

Fig. 8 Lift coefficient along domain size

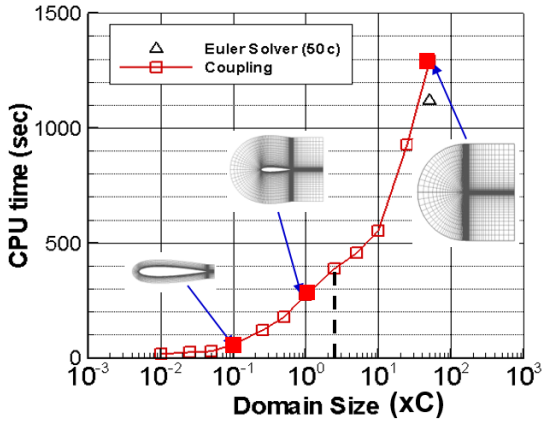

Fig. 9 Computation time along domain size

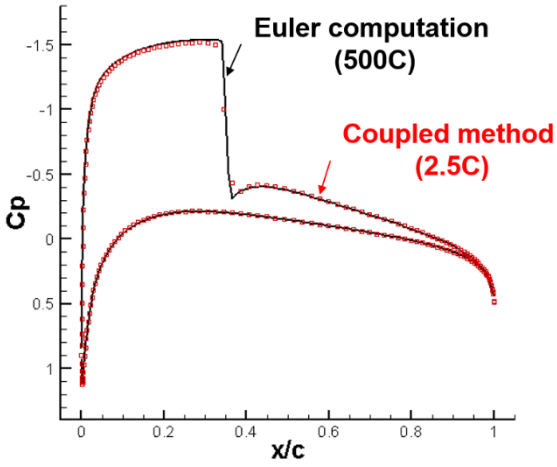

Fig. 10 Comparison of surface pressure distribution

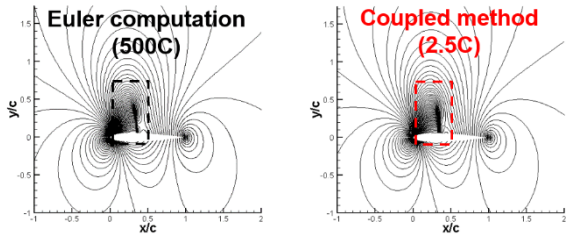

Fig. 11 Comparison of pressure field

3.3 Three-Dimensional NACA 23012 Rectangular Wing at Subsonic Flow ($M = 0.08$, $\alpha = 2, 6, 10°$)

In the third validation case, a rectangular wing with NACA 23012 sectional airfoil and aspect ratio of 6 [7] illustrated in Fig. 12 was considered. The flow condition was Mach number of $M = 0.08$ at various angles of attack of $\alpha = 2, 6, 10°$. For the parameterization of the domain size, a uniform distance along upward, downward, and sideward was used. Fig. 13 shows the examples of the grids with different domain sizes of 128, 0.5 and 0.125 chord lengths. In this validation, the Euler solution with the biggest domain size of 128 chord length was used as the reference for both accuracy and efficiency. In addition, the experimental data [7] was additionally used in the comparison.

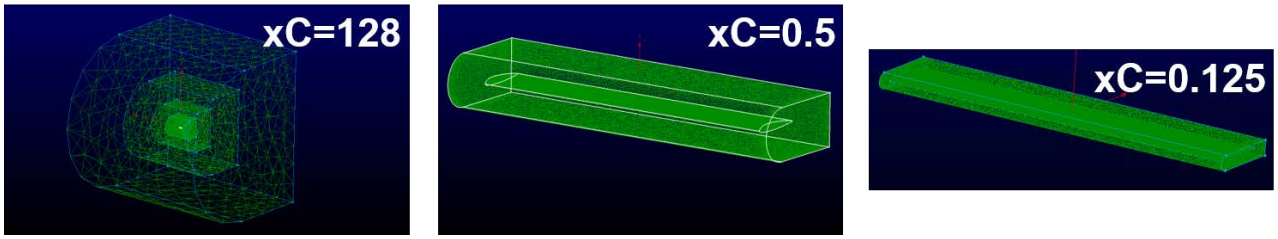

Fig. 13 Examples of grid with different domain sizes

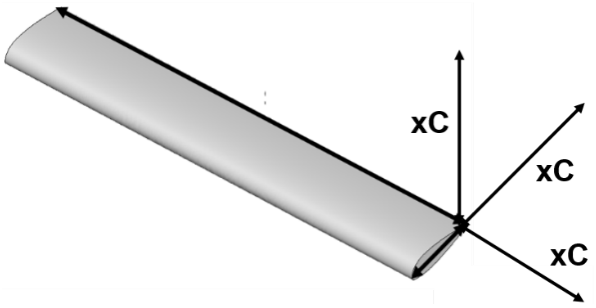

Fig. 12 Schematic of rectangular wing and domain size parameterization

Fig. 14 shows the lift coefficient with respect to angle of attack ($C_L - \alpha$ curve) computed by the reference (blue), the tightly coupled solutions with domain sizes of 0.5 (green) and 0.125 (orange) chord lengths, and the experimental data (black). All of the computation results showed discrepancy compared to the experimental data, and the discrepancy became larger with angle of attack increases. That situation resulted from the flow physics that the flow viscosity cannot be negligible. However, all the computation results showed very good agreement with each other, even at the high angle of attack of $\alpha = 10°$. At that angle of attack, the errors of the coupled solution with domain sizes of 0.5 and 0.125 chord lengths were very small as 0.48% and 0.69%, respectively.

The computation times for the reference and the coupled solutions were 28.1 min., 12.6 min., and 3.0 min., respectively, and that ratio was about 1/9 with the smallest domain size.

Fig. 15 and shows the root sectional surface pressure distributions of the reference (black line) and the coupled solution with the smallest domain size (red dots), and the two pressure distributions showed very good agreement with each other. In addition, Fig. 16 shows the chordwise and spanwise sectional pressure fields near the wing, and it is confirmed that the coupled solver computed very accurate solution even with the small domain size.

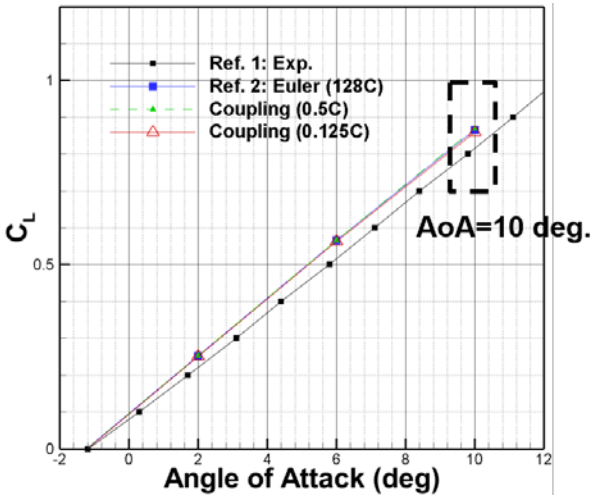

Fig. 14 Comparison of lift coefficient with respect to angle of attack

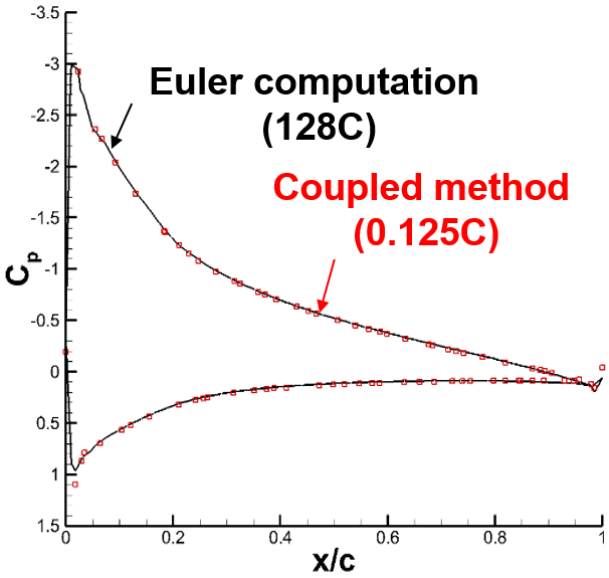

Fig. 15 Comparison of root sectional surface pressure distribution

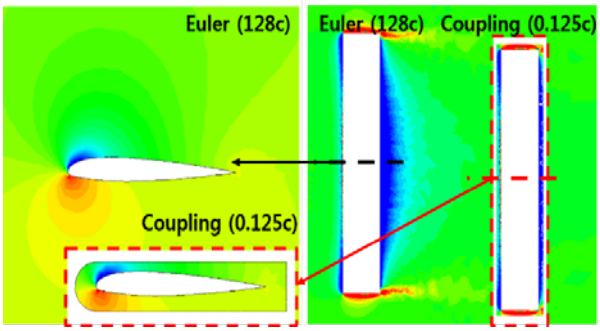

Fig. 16 Comparison of chordwise (left) and spanwise (right) sectional pressure fields

3.4 Three-dimensional ONERA M6 Swept Wing at Transonic Flow ($M = 0.88$, $\alpha = 3.06°$)

The last validation case was the transonic flow around the ONERA M6 swept wing [8], which is well known validation case for the three-dimensional transonic flow. The flow condition was Mach number of $M = 0.88$ at angle of attack of $\alpha = 3.06°$ which generates nonlinear shock waves widely on the upper surface. To determine the domain size, three independent parameters were used for forward, backward, and sideward distances between the wing surface and the domain boundary, respectively, and it is illustrated in Fig. 17. Correspondingly, Fig. 18 shows examples of the grids with different domain sizes., The Euler solution with the grid with biggest domain size of 50x50x50 chord lengths was used as the reference, whereas the two smaller grids of uniform 5x5x5 and non-uniform 3x1x3 chord lengths were used for the tightly coupled solutions.

In order to investigate the accuracy, the lift and drag coefficients were compared. As a result, the errors of the lift coefficients were 0.67% and 1.22% for the coupled solution with domain size of 5x5x5 and 3x1x3 chord lengths, respectively. In case of the drag coefficients, the errors were 0.89% and 0.01%, respectively. The computation times of the reference and the two coupled solutions were 220.0 min., 28.8 min., and 19.9 min., and their ratio were about 1/8 and 1/11, respectively.

Fig. 19, 20, and 21 show the comparisons of the root, mid, and tip sectional pressure distributions, respectively. In each figure, the reference (black line), the coupled solutions with domain sizes of 5x5x5 (blue dots) and 3x1x3 (red dots) chord lengths showed very good agreement with each other.

In conclusion, the tightly coupled solver was well validated in the four cases, and the computation efficiency was improved well with good accuracy, even there were nonlinear shock waves.

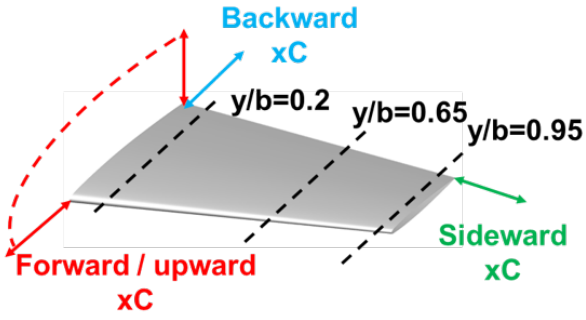

Fig. 17 Schematic of wing and domain size parameterization

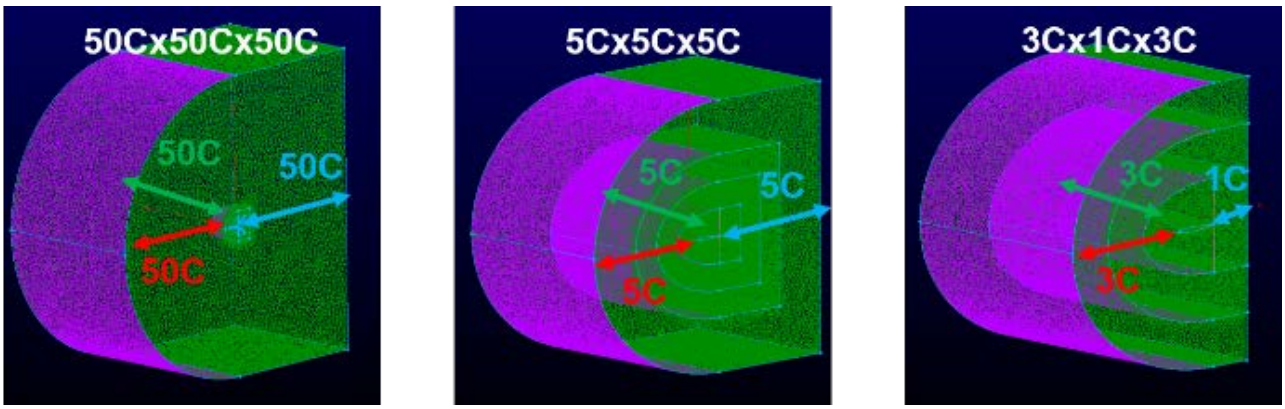

Fig. 18 Example of grids with different domain sizes

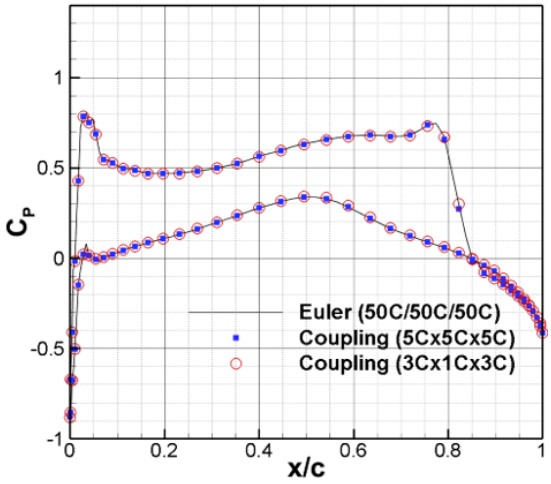

Fig. 19 Comparison of root sectional pressure distribution

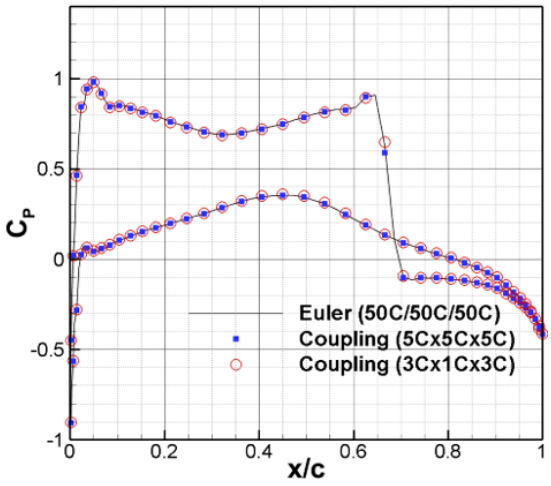

Fig. 20 Comparison of mid sectional pressure distribution

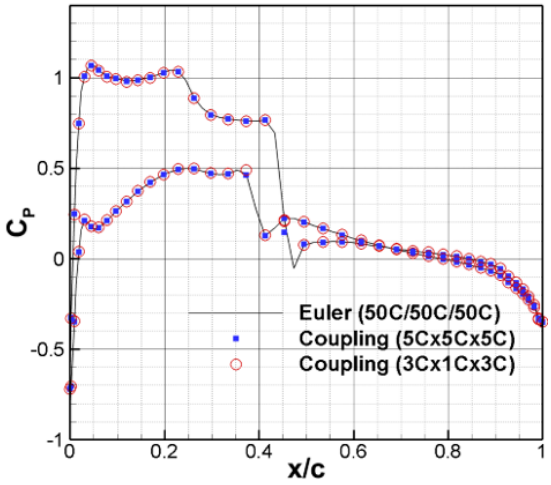

Fig. 21 Comparison of tip sectional pressure distribution

4. Conclusion and Future Work

In the current study, the tightly coupled Euler and potential flow solver was developed to simulate the transonic flows. The coupled solver was validated well in the subsonic and transonic flows around the two-dimensional airfoil and the three-dimensional wings. In the two-dimensional airfoil case, the computation time was reduced to 1/7 at the subsonic flow and 1/3 at the transonic flow, respectively. In case of the three-dimensional wing, the computation time reduced to about 1/10 at both subsonic and transonic flows. The validation results showed that the coupled solver can accurately simulate the linear subsonic and the nonlinear transonic flows within much reduced time.

In the current study, the appropriate domain boundary size was obtained by the repetitive computations with different sizes. For much huger computation efficiency with good accuracy, an adaptive boundary determination method with a proper error indicator will be introduced. Using that method, the boundary size can be varied in the iterative coupling process, and an optimal domain boundary without spoiling the solution will be determined. In addition, to overcome the limitation of the linear propagation of the flow velocity in the nonlinear flow, an appropriate methodology will be devised.

References

[1] Sankar, L. N., Bharadvaj, A. K., and Tsung F. L., Three-dimensional Navier-Stokes/full-potential coupled analysis for viscous transonic flow, *AIAA Journal*, Vol. 31, No. 10, pp 1857-1862, 1993.

[2] Srinivasan, G. R., and Baeder, J. D., TURNS: A free-wake Euler/Navier-Stokes numerical method for helicopter rotors, *AIAA Journal*, Vol. 31, No. 3, pp 959-962, 1993.

[3] Khanna, H., and Baeder, J. D., Coupled free-wake/CFD solutions for rotors in hover using a field velocity approach, *52nd American Helicopter Society (AHS) annual forum*, Washington, D.C., U.S.A., 1996.

[4] Wie, S. Y., Jang, J. S., and Lee, D. J., An analysis for grid reduction for solving rotor blade with CFD/doublet surface/free-wake coupling", *66th American Helicopter Society (AHS) annual forum*, Phoenix, AZ, U.S.A., 2010.

[5] Palacios, F., Colonno, M. R., Aranake, A. C., Campos, A., Copeland, S. R., Economon, T. D., Lonkar, A. K.,

Lukaczyk, T. W., Taylor, T. W. R., and Alonso, J. J., Stanford University Unstructured (SU2): an open-source integrated computational environment for multi-physics simulation and design, 51st *AIAA aerospace science meeting and exhibit*, Grapevine, Texas, U.S.A., 2013.

[6] Baayen, J. H., Vortexje – An open-source panel method for co-simulation, 2012.

[7] Eastman, N. J., and William C. C., Characteristics of the N.A.C.A. 23012 airfoil from tests in the full-scale and variable-density tunnels, *NACA report 530*, 1936.

[8] Schmitt, V. and Charpin, F., Pressure distributions on the ONERA-M6-wing at transonic Mach numbers, *AGARD report AR-138*, 1979.

[9] Jo, Y. M., Park, S. H., Lee, D. J., and Choi, S. I., Development of an efficient three-dimensional tightly coupled Euler/potential solve for transonic flow analysis, *34th AIAA applied aerodynamics conference*, Washington, D.C., U.S.A., 2016.

Copyright Statement